

Composition Determination of Corrosion Products from Downhole Tubular of a Sour Gas Well Using new XRD and WDXRF Procedures and Configurations

Shouwen Shen¹, Quanwen Liu^{2*}, Qiwei Wang³, Yousef M. Salim⁴

^{1,3}Research & Development Center, Saudi Aramco, Saudi Arabia

²School of Petroleum Engineering, Guangdong University of Petrochemical Technology, China

⁴South Area Production Engineering Department, Saudi Aramco, Saudi Arabia

*Corresponding author; Email: quanwenliu64@yahoo.com

Abstract—Corrosion study and control of downhole tubing and casing are critical for the economical and safe operation of oil and gas wells. Chemical composition investigation of corrosion products plays a key role in the identification of the corrosion mechanism and the determination of its root cause. In this study, the analytical techniques of X-ray diffraction (XRD) and wavelength dispersive X-ray fluorescence (WDXRF) spectrometry were used to determine the chemical composition of corrosion products formed on the pulled-out-of-hole (POOH) flow coupling and full joints of a sour gas well in Saudi Arabia. The samples were in the form of metal cuts and could not be prepared with the routine method for XRD and WDXRF analysis. These unconventional samples were handled using an adapted XRD configuration: X-ray point focus rather than line focus and an open eulerian cradle. With the new setup, XRD phase identification and quantification were successfully performed. It was found that the outer diameter surface of the pulled flow coupling and full joints consisted mainly of iron oxides whereas the inner diameter surface consisted mainly of iron sulfides. The XRD findings were further confirmed by WDXRF analysis. The findings suggested that the corrosion products were formed under different conditions.

Keywords—Corrosion products, iron oxide, iron sulfide, XRD analysis, WDXRF analysis.

I. INTRODUCTION

Corrosion is the destructive attack of a material by reaction with its environment^[1] and a natural potential hazard associated with oil and gas production and transportation facilities.^[2] Almost any aqueous environment can promote corrosion, which occurs under numerous complex conditions in oil and gas production, processing, and pipelines systems.^[3] Crude oil and natural gas can carry various high-impurity products which are inherently corrosive. In the case of oil and gas well, such highly corrosive media are carbon dioxide, hydrogen sulfide, and free water.^[4] Continual extraction of carbon dioxide, hydrogen sulfide and free water through oil and gas components can over time make the internal surfaces of these components to suffer from corrosion effects. The lines and their component would undergo material degradations with the varying conditions of the well due to changes in fluid compositions, souring of wells over the period, and changes in operating conditions of the pressures and temperatures. This material degradation results in the loss of mechanical properties like strength, ductility, and so on. This leads to loss of materials, reduction in thickness, and at times ultimate failure.^[5] Therefore, study and control of downhole tubing and casing are critical for the economic and safe operation of oil and gas wells. In this case study, a sour gas producing well in Saudi Arabia was selected for the investigation. This well was put on producing in 2009 and the production has declined over time. Four metal cuts samples were taken out from the downhole tubular (**Table 1**) and the corrosion products were analyzed. In order to investigate the exact composition and nature of the corrosion products, the analytical techniques of X-ray diffraction (XRD) and wavelength dispersive X-ray fluorescence (WDXRF) spectrometry were used.

TABLE 1
SAMPLE INFORMATION

Sample #	#1	#2	#3	#4
Description	Flow coupling inner side	Flow coupling outer side	Joint cut inner side	Joint cut outer side
Picture				

II. EXPERIMENTAL

2.1 Challenges faced

For routine composition analysis using XRD and WDXRF techniques, the samples to be analyzed should be in dry powder status. However, the samples in this study were in the form of metal cuts and could not be ground into powder. Special handling procedures and new instrumental configurations were needed.

2.2 Solution with WDXRF Analysis

X-ray fluorescence spectrometry (XRF) is an analytical technique to determine the elemental composition of various materials. XRF has the advantage of being non-destructive, multi-elemental, fast and cost-effective.^[6, 7] XRF technique can be categorized into two classes: energy dispersive X-ray fluorescence (EDXRF) and wavelength dispersive X-ray fluorescence (WDXRF) spectrometry. The elements that can be analyzed and their detection levels mainly depend on the spectrometer system used. The elemental range for EDXRF goes from sodium (Na) to uranium (U). For WDXRF it is even wider, from beryllium (Be) to uranium (U). The concentration range goes from part per million (ppm) levels to 100%. For routine elemental analysis, the analyzed samples will be ground into powder and pressed into pellet or melt into fusion beads. In this study, all samples were directly put in a special sample holder and measured as-received (metal cuts) in helium atmosphere rather than in vacuum condition. WDXRF data were obtained using Ominion standardless method for elemental composition determination semi-quantitatively with PANalytical Advanced Axios spectrometer.

TABLE 2
WDXRF RESULTS OF METAL CUTS FROM A DOWNHOLE TUBULAR

Element	Flow Coupling Cut		Joint Cut	
	Inner Side (Wt.%)	Outer Side (Wt.%)	Inner Side (Wt.%)	Outer Side (Wt.%)
Fe	70.2	59.5	56.9	53.8
Cr	12.4	3.9	10.8	2.6
S	7.2	0.2	12.6	0.4
Ni	4.0	0.9	4.3	0.4
Mo	1.8	1.2	1.6	1.1
Si	0.6	0.5	0.5	0.5
Al	0.5	0.4	0.3	0.3
Mg	0.5	0.4	0.5	0.5
Ca	0.2	0.6	0.6	8.4
Mn	0.1	0.1	0.2	0.2
Na	0.1	0.1	0.1	0.1
Ba		-	8.5	-

2.3 Solution with XRD Analysis

XRD is a non-destructive technique for analyzing a wide range of materials, including metals, minerals, polymers, catalysts, plastics, pharmaceuticals, thin-film coatings, ceramics, solar cells and semiconductors.^[6, 7] Therefore, XRD has become an indispensable method for materials investigation, characterization and quality control. In this study, XRD analysis was performed on four samples collected from the downhole tubular of a sour gas well. As all samples were in form of metal cuts and they could not be ground into powder with the routine method for XRD analysis. A special XRD configuration (X-Ray point focus rather than line focus) and new setup (using Open Eulerian Cradle) were adapted in order to handle these unconventional samples. With the new setup, XRD phase identification and quantification were successfully performed. The XRD patterns of the metal cuts samples were measured as received using a PANalytical X'Pert PRO PW3050/60 diffractometer (CuK α radiation generated at 45 kV and 40 mA) equipped with an automatic divergence slit, irradiated length of 15 mm, receiving slit size of 0.3 mm, single Xenon detector and an open eulerian cradle with manual Z translation stage for sample directly mounting. The samples were measured from 10 ° to 95 ° 2 θ with a step size of 0.02 °, scan step time 1s. To identify the phases present in the samples, the XRD patterns of the samples were compared with every calculated pattern in the Powder Diffraction File (PDF) database from the International Center for Diffraction Data (ICDD). Using the search-match capabilities of XRD software JADE 9.1+ and the ICDD-PDF database, all phases present in the samples were identified. The quantification of the date was performed by using the Rietveld refinement method.

TABLE 3
XRD RESULTS OF METAL CUTS FROM A DOWNHOLE TUBULAR

Compound	Flow Coupling Cut		Joint Cut	
	Inner Side (Wt.%)	Outer Side (Wt.%)	Inner Side (Wt.%)	Outer Side (Wt.%)
Iron-Fe	98	-	18	-
Troilite-FeS	2	-	-	-
Magnetite-Fe ₃ O ₄	-	99	2	21
Hematite-Fe ₂ O ₃	-	1	-	63
Pyrite-FeS ₂	-	-	40	-
Pyrrhotite-Fe _{1-x} S	-	-	18	-
Barite-BaSO ₄	-	-	22	-
Aragonite-CaCO ₃	-	-	-	16

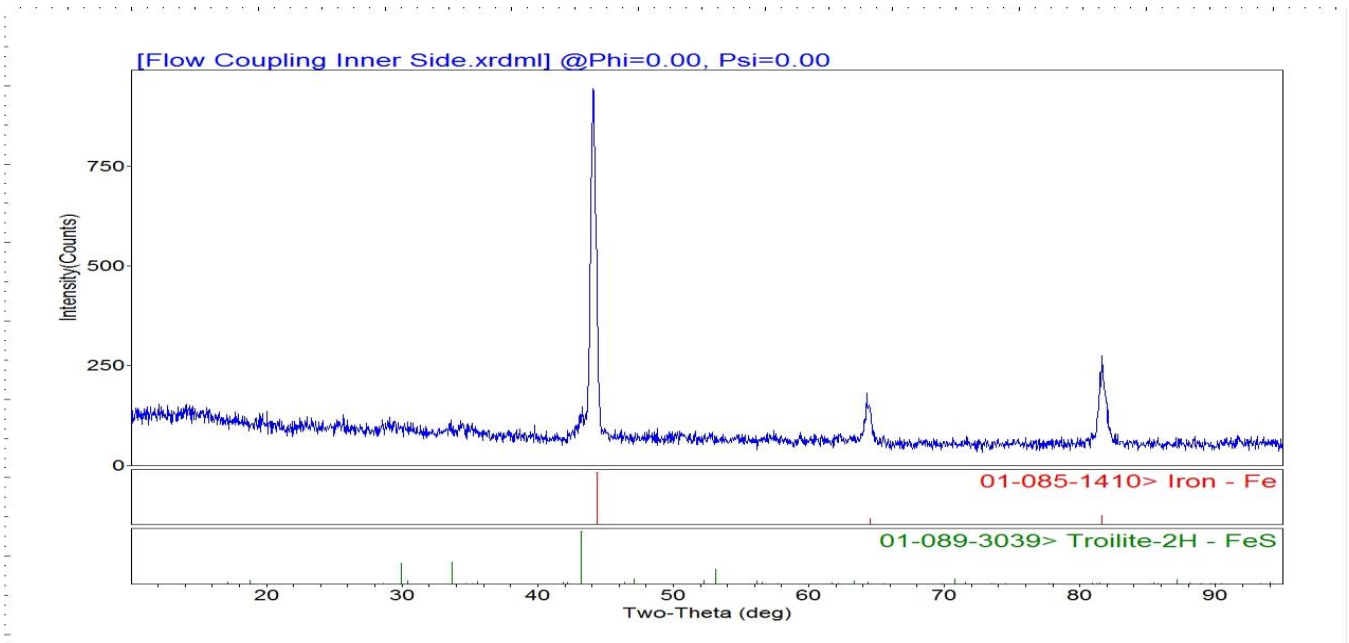


FIG. 1 XRD Pattern of Flow Coupling Inner Side

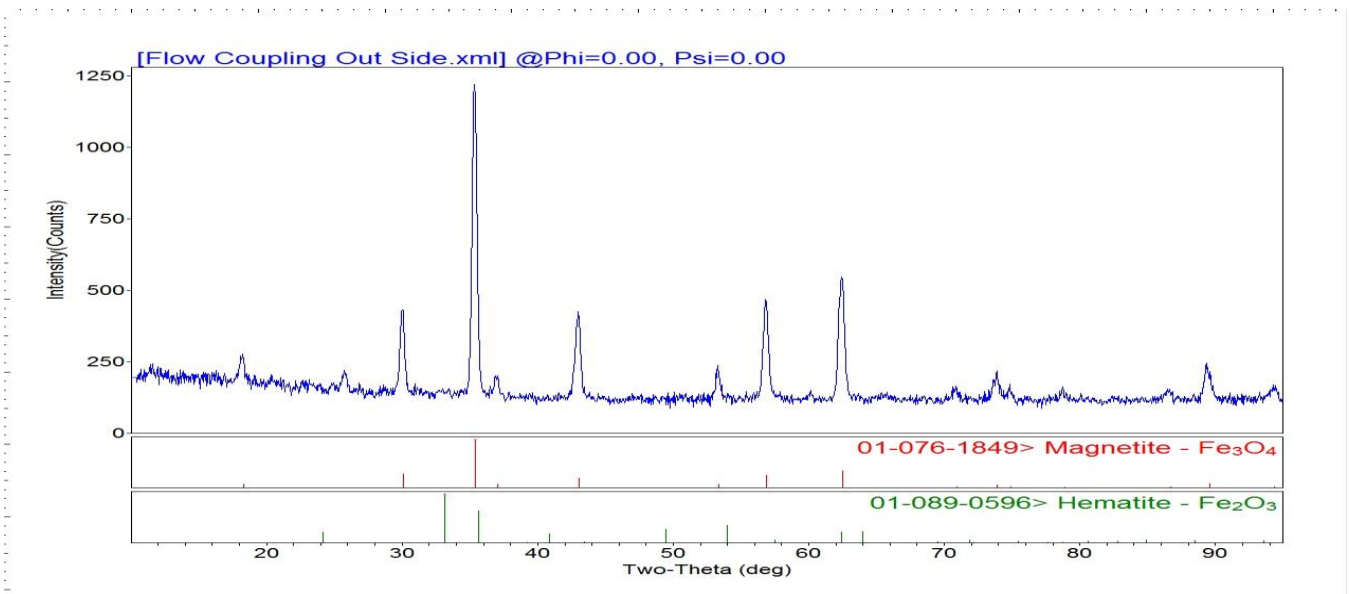


FIG. 2 XRD Pattern of Flow Coupling Out Side

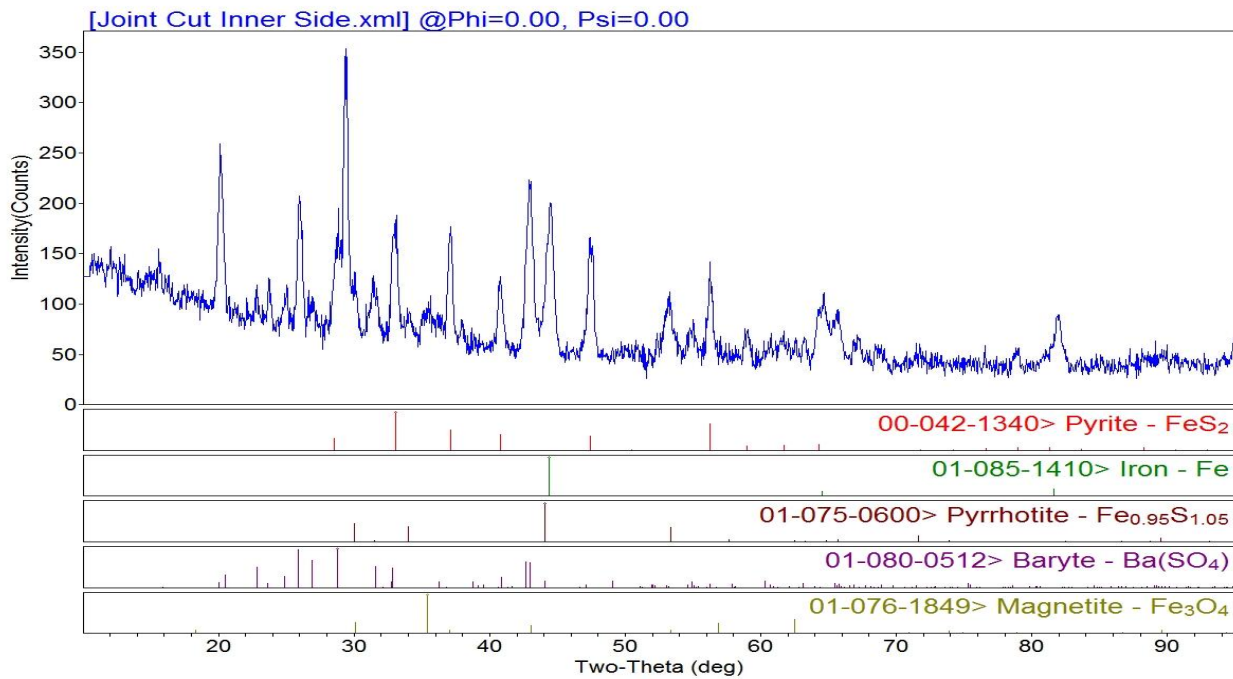


FIG. 3 XRD Pattern of Joint Cut Inner Side

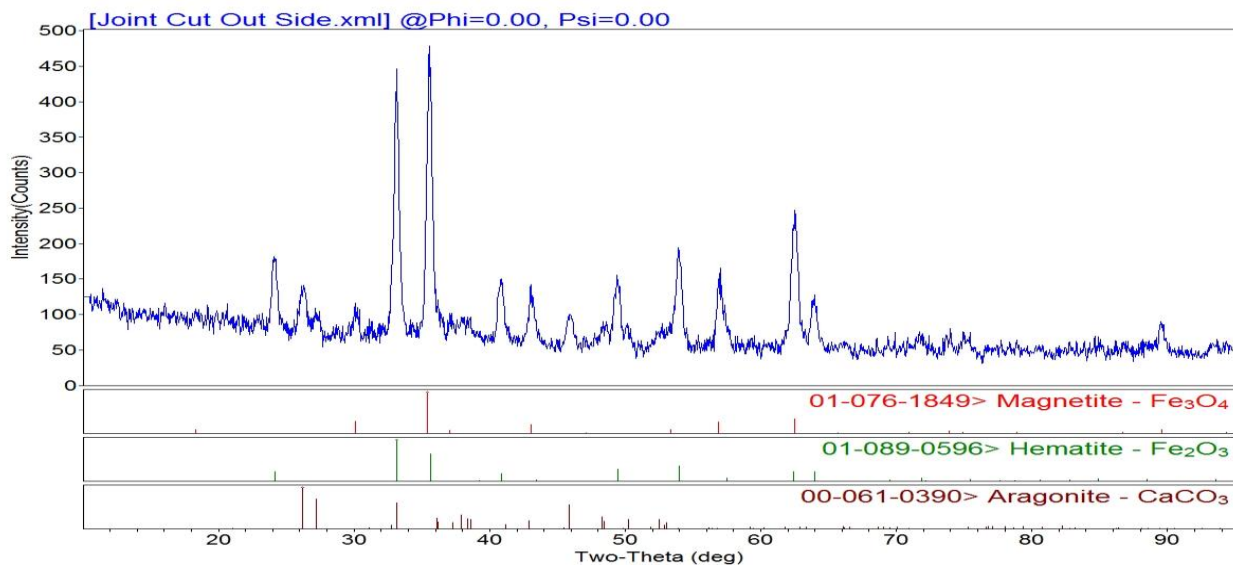


FIG. 4 XRD Pattern of Joint Cut Out Side

III. RESULTS AND DISCUSSION

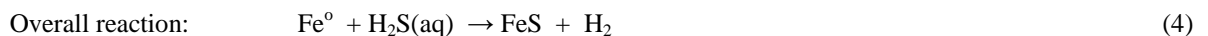
WDXRF results listed in **Table 2** indicate that iron (Fe) is the major element with an average of 60.1% (53.8% to 70.2%). The minor elements are chromium (Cr) with an average of 7.4% (2.6% to 12.4%) and sulfur (S) with an average of 5.1% (0.2% to 12.6%). Other elements such as Ni, Mo, Si, Al, Mg, Ca, Mn, Na, and Ba are also reported in small amounts. The XRD results of the identified compounds are listed in **Table 3** (relative approximate values, normalized to 100%) and the XRD patterns with identified compound references are illustrated in **Fig.1-4**. XRD results showed that the samples consisted mainly of corrosion products in form of magnetite- Fe_3O_4 , hematite- Fe_2O_3 , pyrite- FeS_2 , and pyrrhotite- Fe_{1-x}S with appreciable amounts of scale deposits in form of aragonite- CaCO_3 and barite- BaSO_4 . The original material of iron-Fe was also identified in the inner side samples. XRD results didn't show any chromium (Cr) containing compounds whereas WDXRF analysis

showed the samples contained chromium (Cr) with an average of 7.4% (2.6% to 12.4%). The reason is that Cr and other metal elements such as Ni and Mo etc. can replace Fe partially in iron oxides and iron sulfides. The findings revealed that the corrosion products of the tubular inner side were mainly iron sulfides whereas the corrosion products of the tubular outer side were mainly iron oxides, which indicated they were formed in different conditions. The inner side was exposed to high H₂S fluid and the outer side was in contact with packer fluid which contains no H₂S. Iron oxides usually form under oxidized conditions where dissolved iron is in the form of ferric state. The iron oxides identified in this study could be formed due to residual dissolved oxygen in packer fluid. At high temperatures, iron oxides can also be formed by the oxidation of ferrous iron (Fe²⁺) by H₂O in the absence of H₂S.^[8]



The formation of iron sulfides requires a strictly reducing environment. In fact, iron oxides are unstable in the presence of H₂S and can be quickly converted into iron sulfides.^[9,10]

It is reasonable that the inner side samples had the corrosion products of iron sulfides as the samples were collected from a sour gas well and H₂S reaction with steel (iron-Fe) tubular occurred in the sour gas flow system. Mild steel is susceptible to H₂S attack and iron sulfide is formed as a reaction by-product. This process has been extensively investigated and well documented.^[11-13] The established reactions between iron and H₂S are as follows:



Where FeS represents the iron sulfide by-products formed. Due to the extremely low solubility of iron sulfide minerals, the Fe²⁺ released in reaction (2) is precipitated into solid FeS, as represented in reaction (4), instead of remaining in a dissolved state. The formation and transformation of iron sulfide minerals follow the Ostwald rippling rule.^[14] A brief discussion is provided below.

It is generally believed that mackinawite is the first phase formed in the Fe-S system and the precursor to the formation of other iron sulfide minerals.^[11, 12] Mackinawite is metastable and has the capacity to transform to other iron sulfide phases, such as pyrrhotite, depending on temperature and solution chemistry. Lennie et al. showed that the spontaneous transformation during exposure of dry mackinawite to X-rays and proposed that greigite forms by rearrangement of Fe cations within the cubic close-packed S array of mackinawite.^[15] Schoonen and Barnes determined the conversion rate of mackinawite to hexagonal pyrrhotite at 150-200°C and found that the conversion is accelerated with decreasing solution pH.^[16]

Pyrrhotite is also metastable with respect to iron disulfide pyrite. Qian et al. studied the transformation under hydrothermal conditions with temperature up to 220 °C at vapor-saturated pressures, and found that the reaction proceeded by a dissolution-reprecipitation mechanism under all conditions.^[17] Pyrite formation proceeded by direct replacement of pyrrhotite and, simultaneously, by overgrowth from solution. The overall reaction can be expressed as:



The above reactions are expressed in terms of sulfur addition.^[17] The transformation process can also be achieved by an iron loss mechanism:^[18]



A third pathway is similar to the first pathway but with H₂S is the oxidant.^[19]



Analysis results also showed different inorganic minerals on joint cut and flow coupling. This could be caused by flow dynamics. Flow coupling is a thick-walled tubular component installed in areas of high turbulence. Turbulence can affect precipitation reaction and also change the deposition and erosion of scale minerals on metal surface.^[20,21]

To prevent the formation of iron oxides on the outer side of joint cut and flow coupling, oxygen scavenger should be added in the packer fluid. To minimize the iron sulfide deposition on inner side, use of corrosion inhibitor is often the most cost effective mitigation method.

IV. CONCLUSION

XRD and XRF chemical composition analyses of corrosion samples in the form of metal cuttings require a special instrument configuration. In this study, a special XRD configuration and setup (x-ray point focus rather than line focus, and an open eulerian cradle) were adapted in order to handle these unconventional samples. XRD and XRF techniques have their advantages and disadvantages respectively. Therefore, the combined usage of XRD and XRF is absolutely necessary. Based on the analytical results, it can be concluded that the corrosion products of the tubular inner side were mainly iron sulfides whereas the corrosion products of the tubular outer side were mainly iron oxides, which indicated they were formed in different conditions.

ACKNOWLEDGEMENTS

The authors would like to acknowledge Saudi Aramco for the permission to publish this paper. Special thanks go to X-Ray Lab members for their help in the experiments.

REFERENCES

- [1] P.R. Roberge, Handbook of corrosion engineering, McGraw-Hill, New York, 2000, p. 7-8.
- [2] M.B. Kermani, L.M. Smith, CO₂ corrosion control in oil and gas production design consideration, The Institute of Materials, European Federation of Corrosion Publications, London, 1997, p. 3-4.
- [3] Champion Technologies, Corrosion mitigation for complex environments, Champion Technologies, Houston, 2012, p. 22-23.
- [4] D. Lusk, M. Gupta, K. Boinapally, Y. Cao, Armoured against corrosion, Hydrocarbon Engineering, 2008, 13, p. 115-118.
- [5] L.T. Popoola, A.S. Grema, G.K. Latinwo, B. Gutti, A.S. Balogun, Corrosion problems during oil and gas production and its mitigation, International Journal of Industrial Chemistry, 2013, 4, p. 1-15.
- [6] S. Shen, H. Sitepu, S.A. Hamoud, I.M. Taie, G. Alabedi, A.A. Sharani, B.F. Daajani, Use of XRD and XRF techniques to determine the chemical composition and crystallite size of metal matrix composite materials, Saudi Aramco Journal of Technology, 2010 winter issue, p. 50-55.
- [7] S. Shen, A.M. Sherik, H. Sitepu, S.R. Zaidi, S.A. Hamoud, Chemical composition determination of black powder samples by XRD and XRF, 13th Middle East Corrosion Conference & Exhibition proceedings, 2010, paper No 10096.
- [8] F. Shi, L. Zhang, J. Yang, M. Lu, J. Ding, H. Li, Polymorphous FeS corrosion products of pipeline steel under highly sour conditions, Corrosion Science, 2016, 102, p.103-113.
- [9] R.A. Berner, Sedimentary pyrite formation, American Journal of Science, 1970, 268, p. 1-23.
- [10] S.W. Poulton, M.D. Krom, J. Van Rijn, R. Raiswell, The use of hydrous iron (III) oxides for the removal of hydrogen sulphide in aqueous systems, Water Research, 2002, 36, p. 825-834.
- [11] S.N. Smith, M.W. Joosten, Corrosion of carbon steel by H₂S in CO₂ containing oilfield environments, CORROSION 2006, paper no. 06115 (Houston, TX: NACE, 2006).
- [12] A.G. Wikjord, T.E. Rummery, F.E. Doern, D.G. Owen, Corrosion and deposition during the exposure of carbon steel to hydrogen sulphide-water solutions, Corrosion Science, 1980, 20, 5, 6, p. 51-671.
- [13] S.N. Smith, B. Brown and W. Sun, Corrosion at higher H₂S concentrations and moderate temperatures, CORROSION 2011, paper no. 11081 (Houston, TX: NACE, 2011).
- [14] J.W. Morse, W.H. Casey, Ostwald processes and mineral paragenesis in sediments, American Journal of Science, 1988, 288, p. 537-560.
- [15] A.R. Lennie, S.A.T. Redfern, P.E. Champness, C.P. Stoddart, P.F. Schofield, D.J. Vaughan, Transformation of mackinawite to greigite: an in situ X-ray powder diffraction and transmission electron microscope study, American Mineralogist, 1997, 82, p. 302-309.
- [16] M.A.A. Schoonen and H.L. Barnes, Mechanisms of pyrite and marcasite formation from solution: III. Hydrothermal processes. Geochim. Cosmochim. Acta, 1991, 55, p. 3491-3504.
- [17] G. Qian, F. Xia, J. Brugger, W.M. Skinner, J. Bei, G. Chen and A. Pring, Replacement of pyrrhotite by pyrite and marcasite under hydrothermal conditions up to 220 °C: An experimental study of reaction textures and mechanisms, American Mineralogist, 2011, 96, p. 1878-1893.
- [18] R.T. Wilkin and H.L. Barnes, Pyrite formation by reactions of iron monosulfides with dissolved inorganic and organic sulfur species, Geochim. Cosmochim. Acta, 1996, 60, p. 4167-4179.
- [19] E. Drobner, H. Huber, G. Wachterhauser, D. Rose and K.O. Stetter, Pyrite formation linked with hydrogen evolution under anaerobic conditions, Nature, 1990, 346, p. 742-744.

-
- [20] L. Sutherland, C. Johnston and W. Taylor, The influence of turbulence (or hydrodynamic effects) on barium sulphate scale formation and inhibitor performance, 2013, SPE International Symposium on Oilfield Chemistry, paper no. 164070.
- [21] A. Quddus and L. Al-Hadhrami, Influence of solution hydrodynamics on the deposition of CaSO_4 scale on aluminum, Journal of Thermophysics and Heat Transfer, 2011, 25, p. 112-118.